Nuclear parameter inference with semi-agnostic priors

Lami Suleiman *
Deutsches Elektronen-Synchrotron DESY, Platanenallee 6, 15738 Zeuthen, Germany and Deutsches Zentrum für Astrophysik (DZA), Postplatz 1, 02826 Görlitz, Germany

Anthea F. Fantina
Grand Accélérateur National d'Ions Lourds (GANIL), CEA/DRF - CNRS/IN2P3, Boulevard Henri Becquerel, 14076 Caen, France

Francesca Gulminelli
Université de Caen Normandie, ENSICAEN, CNRS/IN2P3, LPC Caen UMR6534, F-14000 Caen and Institut Universitaire de France (IUF), France

Jocelyn Read
Nicholas and Lee Begovich Center for Gravitational Wave Physics and Astronomy, California State University Fullerton, Fullerton, California 92831, USA

Background: Radio pulsar timing, X-ray pulse profile modeling or gravitational-wave detections of binary mergers involving at least one neutron star offer the opportunity to elucidate the properties of dense and neutron rich matter in thermodynamic regimes inaccessible to nuclear laboratories. Such inference relies on building appropriate equation-of-state priors, such as the recently introduced semi-agnostic constructions that incorporate nuclear theory and experimental information available in low to intermediate density regimes, while offering the necessary flexibility at high density.

Purpose: In this paper, we assess how detections of mass, radius, and tidal deformability for low-mass ($\sim 1M_{\odot}$) or high-mass ($\sim 1.9M_{\odot}$) neutron stars would contribute to constraining nuclear empirical parameters in an inference based on semi-agnostic equation-of-state priors.

Methods: We first assessed the correlation factors between nuclear empirical parameters and the zero-temperature and β-equilibrated pressure in different regimes of density. We then simulate observations for three nucleonic equations of state to test the recovery of the corresponding nuclear empirical parameters.

Results: We show that not all nuclear empirical parameters significantly correlate with the pressure and find a competition between them in the high-density regime that challenges their inference. We also find that using semi-agnostic constructions instead of assuming a nucleonic content up to the highest densities in the neutron-star core can help recover more accurately the true nuclear empirical parameters.

Conclusion: Parameterizing the high-density regime of the equation of state with the nucleonic meta-model can pollute the inference of nuclear empirical parameters; semi-agnostic constructions are a solution to that. However, many nuclear matter empirical parameters contribute in a similar way to the building of baryonic pressure. We find that they are difficult to infer independently even with extremely precise measurements.

I. INTRODUCTION

Observations of neutron stars (NSs) can be used to explore the properties of dense matter under extreme conditions. The deepest layers of those compact objects harbor densities that exceed several times nuclear saturation density, reaching values well beyond the thermodynamic regimes explored by nuclear theory and experiments on Earth. Astrophysical features of NSs depend on the star internal-matter properties. By comparing the NS-modeled macroscopic parameters to measurements extracted from multi-messenger observations, the properties of strong interaction in (relatively) cold temperature and high-density regimes are expected to be constrained.

A variety of signals emitted by NSs have already provided valuable information on their internal structure. The timing of the pulsation in radio emitted by the magnetic field of rotating NSs has permitted very accurate measurements of their mass (see e.g., Özel and Freire [1]). The existence of high-mass pulsars such as PSR J0740+6620 [2] requires that the pressure provided by matter in the high-density core of the star be sufficiently large to support the star against self-gravitational collapse. Gravitational waves emitted during the merger of two compact objects keep the imprint of the mass and the deformation of the binary objects in the presence of an external gravitational field [3]. The detection of the Binary neutron star (BNS) merger GW170817 [4] has shown a preference for a small induced quadrupolar moment in response to an external tidal field, thus excluding high pressures in the NS core, see Refs. [5–9] and references therein. Using the relativistic effects revealed

* lami.suleiman@desy.de

by the x-ray signal emitted by hot spots at the surface of millisecond pulsars, it is possible to measure the mass and radius of NSs simultaneously [10]. The Neutron Star Interior Composition ExploRer (NICER) published mass-radius posterior contours as well as EoS constraints for several sources (PSR J0030+0451 [11, 12], PSR J0740+6620 [13, 14], PSR J0437−4715 [15]); the source PSR J0437-4715 presented EoS constraints consistent with GW170817. All these properties can be directly mapped to the equation of state (EoS) of cold and β-equilibrated dense matter, even if they are not yet sufficient to firmly establish the composition of matter at high density. The sensitivity expected for the third generation (3G) of gravitational wave detectors (Cosmic Explorer [16–18] and Einstein Telescope [19–21]) promises a large increase in the number of BNS merger detections and in the precision of the compact-object properties [20, 22]. The new Advanced Telescope for High-ENergy Astrophysics (ATHENA) mission [23] is expected to detect soft x-rays emitted by millisecond pulsars, offering unprecedented spectral and time resolution to determine the atmosphere composition, mass and radius of NSs, including for sources that are currently considered faint. An increase in the number of observed sources and in the accuracy of NS macroscopic parameter measurements will help us constrain dense-matter properties significantly.

Aside from constraining the EoS, it may also be possible to constrain nuclear empirical parameters (NEPs [24]), such as the nuclear saturation density, the symmetry energy or the incompressibility, with future NS observations. In Iacovelli et al. [25], using simulated gravitational-wave data in the context of 3G detector sensitivity, the authors present to what extent it will be possible to constrain NEPs using an EoS prior based on the meta-modeling approach (see Margueron et al. [26] and reference therein). They highlight a degeneracy in the determination of NEPs that manifests as multi-peaked posterior distributions, even when informed by a large number of precise astrophysical detections. Similar conclusions were discussed for example in Refs. [9, 27, 28].

In this paper, we discuss the performance of EoS and NEP inference using the semi-agnostic EoS construction presented in Davis et al. [29], that is, a meta-modeling approach coupled with a polytrope extension at high density. Section II details the methods used in this paper: the semi-agnostic EoS model is first introduced in Section II A, brief details on the NS macroscopic parameter modeling are presented in Section II B, and Section II C presents the simple approach taken to simulate high-precision detection with a non correlated bivariate Gaussian distribution. Section III is dedicated to the results of our analysis: the EoS prior sets used for the inference, their corresponding astrophysical parameters, as well as details on the NEPs, are presented in Section III A, while we discuss in Section III B 2 the NEP constraints obtained from simulated data. Additional discussions and conclusions are given in Sects IV and V, respectively.

II. METHODS

A. Semi-agnostic equation of state model

The EoS construction follows the semi-agnostic (SA) approach discussed in Davis et al. [29]: in the low-density regime, $n = [10^{-11}\mathrm{fm}^{-3}; n_{\mathrm{match}}]$, the EoS is based on the meta-model introduced in Margueron et al. [26], and in the high-density regime, $n = [n_{\mathrm{match}}; n_{\mathrm{max}}]$, the EoS is based on piecewise polytropes. The different sets used in this paper were generated with `CUTER`[1]. We refer to Davis et al. [29] and references therein for a detailed description of the SA model, and briefly review the construction of this model in the following sections.

1. Low-density construction: the meta-model

The zero-temperature and β-equilibrated low-density EoS of homogeneous matter composed of neutrons n, protons p, electrons e, and muons μ ($npe\mu$ matter) was calculated using the nucleonic meta-model approach. The latter model is a non-relativistic flexible parametrization of the baryonic part of the energy density, in the hypothesis that baryonic matter is solely constituted of neutrons and protons, with respective masses m_q and densities n_q ($q = n, p$). The baryonic energy density reads

$$\begin{aligned}\epsilon_{\mathrm{nuc}}(n,\delta) = (m_n n_n + m_p n_p)c^2 + \epsilon^*_{\mathrm{FG}}(n,\delta) \\ + \epsilon_{\mathrm{is}}(n) + \epsilon_{\mathrm{iv}}(n)\delta^2 \ , \end{aligned} \tag{1}$$

with c the speed of light, $n = n_n + n_p$ the baryon density and $\delta = (n_n - n_p)/n$ the isospin asymmetry. The interaction part of the baryonic energy density for symmetric matter (composed of equal number of neutrons and protons) is denoted ϵ_{is} and is also referred to as the isoscalar energy. The symmetry energy density (or isovector energy) quantifies the energy required by the system to transform isospin symmetric matter into pure neutron matter. The interaction contribution to the symmetry energy is noted ϵ_{iv}, while a first-order correction to the parabolic expansion in δ is given by the kinetic term, with a functional form given by the free Fermi gas:

$$\epsilon^*_{\mathrm{FG}}(n,\delta) = \epsilon^*_{\mathrm{FG}}(n,\delta; n_{\mathrm{sat}}, m^*_{\mathrm{sat}}, \Delta m^*_{\mathrm{sat}}) \ . \tag{2}$$

[1] A publicly available version of the Crust (Unified) Tool for Equation-of-state Reconstruction (`CUTER`) is accessible on the Zenodo repository [30].

The nuclear saturation density, denoted $n_{\rm sat}$, is the baryon density at the nuclear saturation point, that is to say the density defined by the minimum value of the energy per baryon in symmetric matter. The Landau nucleon effective mass at nuclear saturation density in symmetric matter is denoted $m^*_{\rm sat}$. The effective mass isospin splitting (or isosplit), denoted $\Delta m^*_{\rm sat}$, is defined at nuclear saturation as the difference between the neutron and proton Landau effective mass in pure neutron matter, see Eq. (6) of Margueron et al. [26].

Both the isoscalar and isovector terms of the baryonic energy densities, $e_{\rm is}$ and $e_{\rm iv}$, are formulated as a fourth-order truncated Taylor expansion around $n_{\rm sat}$. Each order of the Taylor expansion is associated to a different NEP that also contains contributions from the density dependence of the effective masses: We denote $X_{\rm is}$ and $X_{\rm iv}$ the ensemble of isoscalar and isovector NEPs, respectively,

$$\{X_{\rm is}\} = \{E_{\rm sat}, K_{\rm sat}, Q_{\rm sat}, Z_{\rm sat}\} \ , \tag{3}$$
$$\{X_{\rm iv}\} = \{E_{\rm sym}, L_{\rm sym}, K_{\rm sym}, Q_{\rm sym}, Z_{\rm sym}\} \ . \tag{4}$$

NEPs are defined at saturation density, with E denoting the energy, L the slope of the energy, K the incompressibility, Q the skewness and Z the kurtosis; the definition of the nuclear saturation point implies $L_{\rm sat} = 0$. The isoscalar and isovector baryonic energy densities depend on $X_{\rm is}$ and $X_{\rm iv}$, respectively, as

$$\epsilon_{\rm is}(n) = \epsilon_{\rm is}(n; n_{\rm sat}, \{X_{\rm is}\}, m^*_{\rm sat}, \Delta m^*_{\rm sat}, b) \ , \tag{5}$$
$$\epsilon_{\rm iv}(n) = \epsilon_{\rm iv}(n; n_{\rm sat}, \{X_{\rm iv}\}, m^*_{\rm sat}, \Delta m^*_{\rm sat}, b) \ ; \tag{6}$$

for details on the explicit formulas of $\epsilon_{\rm is}$ and $\epsilon_{\rm iv}$, we refer to Eqs. (16)-(24) of Davis et al. [29] or to Eqs. (22)-(31) of Margueron et al. [26]. The parameter b enters in the correction term to the potential energy, that ensures the correct zero-density limit; see Eq. (37) in Margueron et al. [26]. It has a negligible influence on the results presented in this paper.

As the meta-model parametrizes only the baryonic contribution to the homogeneous-matter energy density, the contribution of leptons is added to build the EoS of $npe\mu$ matter. As for the inhomogeneous matter in the crust, the cold compressible liquid drop model was used for the ions. In this approach, the cluster bulk energy (described within the meta-model) is complemented with the Coulomb interaction and the residual interface interaction between the nucleus and the surrounding dilute nuclear-matter medium, as described in Davis et al. [29], Carreau et al. [31]. The parameters entering the cluster surface energy were determined to reproduce the experimental nuclear masses in the 2020 Atomic Mass Evaluation (AME) table [32]. The unified EoS was then obtained variationally, under the constraints of baryon number conservation and charge neutrality. The pressure P was calculated using standard thermodynamic relations from the energy density, $\epsilon(n)$.

Causality is imposed *a posteriori* on the meta-model EoS: models that present supraluminal sound speeds before $n_{\rm match}$ are rejected. To impose chiral effective field theory (χ-EFT) constraints, we also compute the zero-temperature baryonic energy density for pure neutron matter, $e_{\rm nuc}(n, \delta = 1)$, in the density interval $n \in [\min(n_{\chi\rm data}), \min(n_{\rm match}, \max(n_{\chi\rm data}))]$, with $n_{\chi\rm data}$ the range of baryonic density at which χ-EFT data is provided. Instead of using the earlier Drischler et al. [33] constraint as in Davis et al. [29], we applied an updated constraint in the range $n_{\chi\rm data} \in [0.02; 0.2]$ fm^{-3} that is based on the range of results compiled by Huth et al. [34][2].

The meta-model is abandoned beyond $n_{\rm match}$ in favor of a more agnostic approach for the following reasons: (i) the Taylor expansion around nuclear saturation density $n_{\rm sat}$ fails for large density values [26], and (ii) the purely nucleonic degrees of freedom on which the meta-model is based on might not be correct in the high-density regime, because it has been hypothesized that the core of NSs may gather more exotic particles such as hyperons (see e.g., Vidaña [35], Oertel et al. [36]) or deconfined quarks (see e.g., Baym et al. [37]).

2. *High-density construction: piecewise polytropes*

Beyond $n_{\rm match}$, we used the agnostic formulation of piecewise polytropes, see Read et al. [38], that is, the pressure and rest-mass density $\rho = n m_n$ (with m_n the nucleon mass) are related according to the formula $P = \kappa\rho^\gamma$, with κ being the polytropic constant and γ the adiabatic index. We used $N = 5$ polytropes defined by $\{\gamma_i, \kappa_i, \rho^{\rm tr}_{i-1}\}$, with $\rho^{\rm tr}_{i-1}$ the transition density between the polytropes and $i \in [1; N]$. The first polytrope was matched with the low-density meta-model EoS at $\rho^{\rm tr}_0 = \rho_{\rm match} = m_n n_{\rm match}$, and pressure continuity was ensured at all transition densities between the polytropes. Therefore, the high-density EoS is entirely known if we specify $n_{\rm match}$, 5 adiabatic indices and 4 transition densities. We computed $P(n)$ and $P(\epsilon)$ in the density range $[n_{\rm match}; \max(n_{\rm cs}, 20n_0)]$, with $n_0 = 0.16$ fm^{-3} and $n_{\rm cs}$ the maximum baryon density that ensures causality of the polytropic extension, because polytropes are not causal by construction.

3. *Equation-of-state prior sets*

NEPs were sampled along a uniform distribution, in intervals presented in Table I, to compute the low-

[2] The implementation of this constraints was done as follows: the energy per nucleon of pure neutron matter predicted by each (meta-)model is compared with the energy bands in Huth et al. [34] (see their Fig. 4), enlarged by 5%. Models not consistent with the $\chi-$EFT band are discarded.

Parameter X	X_{min}	X_{max}
n_{sat} [fm^{-3}]	0.14	0.17
E_{sat} [MeV]	-17.0	-15.0
K_{sat} [MeV]	190	290
Q_{sat} [MeV]	-1000	1000
Z_{sat} [MeV]	-3000	3000
E_{sym} [MeV]	26	38
L_{sym} [MeV]	10	80
K_{sym} [MeV]	-400	200
Q_{sym} [MeV]	-2000	2000
Z_{sym} [MeV]	-5000	5000
m^*/m	0.6	0.8
$\Delta m^*/m$	0.0	0.2
b	1	10

TABLE I: Bounds in which the meta-model nuclear parameters X are sampled. The mean effective mass and effective isosplit are normalized to $m = \frac{m_n+m_p}{2}$.

density EoS ($n \in [10^{-11}$ fm^{-3} ; $n_{\mathrm{match}}]$). The lower and upper boundaries chosen for n_{sat} , E_{sat} , K_{sat} , E_{sym} , L_{sym} and K_{sym} were inspired by various nuclear experiments (see e.g., Oertel et al. [39], Le Fèvre et al. [40], Danielewicz et al. [41]); the intervals for n_{sat} and K_{sat} were extended to accommodate values for equations of state discussed in Sect. II C. It is important to stress that, although the NEPs were sampled with a flat distribution, their resulting prior distribution is not necessarily flat because of the constraints associated to causality and the existence of a viable crust.

The adiabatic indices γ and transition densities ρ^{tr} for the piecewise polytropes were sampled along a uniform distribution in intervals $\gamma \in [0, 8]$ and $[\rho_{\mathrm{match}}, 10 n_0 m_n]$ respectively. With the `CUTER` code, we prepared 4 different sets:

- SA-Exp-n$_0$: follows the semi-agnostic approach discussed in this section, with the meta-model construction extending up to $n_{\mathrm{match}} = n_0 = 0.16$ fm^{-3} . This set is solely informed by nuclear experiments which have guided the limits of the NEPs priors.

- SA-Exp-2n$_0$: similar to SA-Exp-n$_0$ but with $n_{\mathrm{match}} = 2n_0 = 0.32$ fm^{-3} .

- SA-χ-n$_0$: similar to SA-Exp-n$_0$ ($n_{\mathrm{match}} = n_0$) with the addition of χ-EFT constraints imposed for $n \in [\min(n_{\chi\mathrm{data}}); n_0]$.

- MM-χ : the low density meta-model is extended at high density instead of using piecewise polytropes. χ-EFT constraints are imposed for $n \in [\min(n_{\chi\mathrm{data}}) - \max(n_{\chi\mathrm{data}})] = [0.02 - 0.2]$ fm^{-3} .

The sets comprised 5×10^4 EoSs each and were used as *priors* to a Bayesian inference with astrophysical data.

B. Neutron-star astrophysical parameters

For each EoS of the sets, the NS total mass M, total radius R, and dimensionless tidal deformability Λ were modeled in the framework of general relativity. The mass-radius sequence for each EoS was computed by solving Einstein's equations for a static metric (Tolman-Oppenheimer-Volkov equations [42, 43]), while varying the central energy density of the star.

The dimensionless tidal deformability is defined as

$$\Lambda = \frac{2}{3} k_2(r = R) \left(\frac{Rc^2}{GM} \right)^5 , \tag{7}$$

with $k_2(r)$ the second-order tidal Love number. The quantity k_2 is the solution of ordinary differential equations presented in Hinderer [44], which were solved simulateneously with the Tolmann-Oppenheimer-Volkov equations.

C. Simulated astrophysical data

In this paper, we simulate data on M, R and Λ and study the recovery of the EoS and NEPs through inference. Three injection nucleonic EoSs that are unified[3] and available on CompOSE [45] were used to simulate the data: RG(SLY2) [46], PCP(BSK24) [47] and GPPVA(NL3$\omega\rho$) [48]; nuclear and astrophysical properties of the injection EoSs are presented in Table II.

Contrary to Boudon et al. [49] and Iacovelli et al. [25], we did not perform a full population study to simulate the astrophysical data in this paper. Rather, we focused on simulating NS sources detected with high precision and at extremes of the plausible mass range for astrophysical neutron stars to test the limits of EoS and NEP inference capabilities. For each injection EoS, we assumed the detection of the mass, radius and tidal deformability for:

- 10 NS sources with uniformly distributed masses $M_{\mathrm{source}} \in [0.9 - 1.1]$ $\mathrm{M}_\odot$: this ensemble of NS sources is referred to as "small-mass" sources;

- 10 NS sources with uniformly distributed masses $M_{\mathrm{source}} \in [1.8 - 2.0]$ $\mathrm{M}_\odot$: this ensemble of NS sources is referred to as "high-mass" sources.

For each NS source, we simulated the detection using a non-correlated bivariate Gaussian distribution centered on $\left(M_{\mathrm{source}}, X^{\mathrm{inj}}(M_{\mathrm{source}})\right)$ with $X = R, \Lambda$ and X^{inj} determined by the injection EoS; the ensemble of K simulated data points $\{M^K_{\mathrm{source}}, X^K(M_{\mathrm{source}})\}$

[3] The core and the crust of a unified EoS are calculated consistently using the same nuclear model.

	RG(SLy2)	PCP(BSk24)	GPPVA(NL3-$\omega\rho$)
	Astro. for $M = (1.0, 1.4, 2.0)$ $M_\odot$		
n_c [fm^{-3}]	(0.407, 0.530, 0.941)	(0.331, 0.407, 0.589)	(0.256, 0.293, 0.358)
P_c [MeV/fm^3]	(37.8, 82.7, 428.7)	(28.6, 55.5, 165.8)	(20.4, 35.0, 73.6)
R [km]	(11.91, 11.76, 10.71)	(12.46, 12.58, 12.31)	(13.52, 13.81, 14.09)
Λ	(2342.4, 310.0, 11.3)	(3279.2, 518.9, 40.6)	(5081.7, 944.3, 119.8)
	Nuclear empirical parameters		
n_{sat} [fm^{-3}]	0.161	0.1578	0.148
E_{sat} [MeV]	-15.99	-16.048	-16.24
K_{sat} [MeV]	229.92	245.5	270.0
Q_{sat} [MeV]	-	-274.5	-198.0
Z_{sat} [MeV]	-	1184.15	-
E_{sym} [MeV]	32.0	30.0	31.7
L_{sym} [MeV]	47.46	46.4	55.0
K_{sym} [MeV]	-115.13	-37.6	-8.0
Q_{sym} [MeV]	-	710.86	-
Z_{sym} [MeV]	-	-4031.3	-

TABLE II: Central baryon density n_c, central pressure P_c, radius R, and tidal deformability Λ at $M = 1.0, 1.4, 2.0$ $M_\odot$, as well as available nuclear empirical parameters of the underlying nuclear models for the RG(SLY2), PCP(BSK24), and GPPVA(NL3$\omega\rho$) EoSs.

was generated according to the standard deviation $(\sigma_M, \sigma_X) = (M_{\rm source}, X^{\rm inj}(M_{\rm source}) \times \delta E$, with $\delta E = 1\%$. Using the probability density function method embedded in the package STATS.MUTLTIVARIATE_NORMAL of the SCIPY library [50], we affected to each EoS of the set a likelihood $\mathcal{L}^{\rm eos}_{\rm source}$ for each NS source given the ensemble of data points $\{M^K_{\rm source}, X^K(M_{\rm source})\}$. Finally, we determined the likelihood $\mathcal{L}^{\rm eos}$ for each EoS of the set given the 10 NS detections by multiplying the likelihood per source.

We acknowledge that the proposed small error δE does not accurately reflect the precision offered by the next generation of detectors, nor the fact that the different observables are affected by very different systematics; moreover, the bivariate Gaussian distribution does not correctly take into account the correlation between NS macroscopic parameters. This simplistic approach was used to test the capabilities of the semi-agnostic EoS sets to recover injection values.

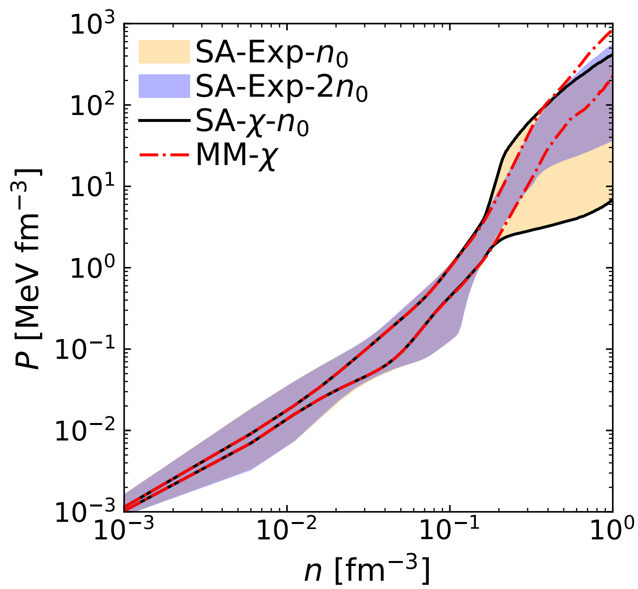

FIG. 1: Pressure P as a function of the baryon density n (90 % contours) for the EoS sets discussed in this paper.

III. RESULTS

A. Priors

1. *Equation of state*

The 90% contours for the pressure-density distribution of the four EoS sets generated with CUTER (see Section II A for details) are presented in Fig. 1, and the corresponding pressure range δP (on the 90% contours) explored by each set is presented in Table III for various values of the baryon density.

For $n \in [10^{-3}; 0.1]$ fm^{-3} , χ-EFT filters constrain significantly the range of pressure explored by the meta-model. In $n \in [0.1 - 0.16]$ fm^{-3} , all four sets approximately converge in terms of δP, with or without χ-EFT filters applied: although the χ-EFT calculations considered extend up to $n = 0.2$ fm^{-3} , the error bar on the χ-EFT data for $n > 0.1$ fm^{-3} is significant, and the pressure range is not constrained beyond nuclear experimental data intervals from which the meta-model EoSs are sampled.

For $n \in [0.16; 0.32]$ fm^{-3} , the sets MM-χ (full meta-model with χ-EFT constraints) and SA-Exp-2n_0 (semi-agnostic with $n_{\rm match} = 0.32$ fm^{-3} without

Set	$\delta P(n_0/10)$	$\delta P(n_0/2)$	$\delta P(n_0)$	$\delta P(2n_0)$	$\delta P(4n_0)$	$\delta P(6n_0)$
SA-Exp-n_0	0.05	0.59	2.8	64.5	223.2	384.9
SA-Exp-2n_0	0.05	0.58	2.7	39.6	240.8	480.7
SA-χ-n_0	0.01	0.30	2.6	64.8	226.0	391.5
MM-χ	0.01	0.30	2.4	41.5	239.0	575.4

TABLE III: 90% contour pressure range $\delta P(n)$ in MeV/fm^3 calculated at $n_0/10$, $n_0/2$, n_0, $2n_0$, $4n_0$ and $6n_0$ for the EoS sets discussed in this paper.

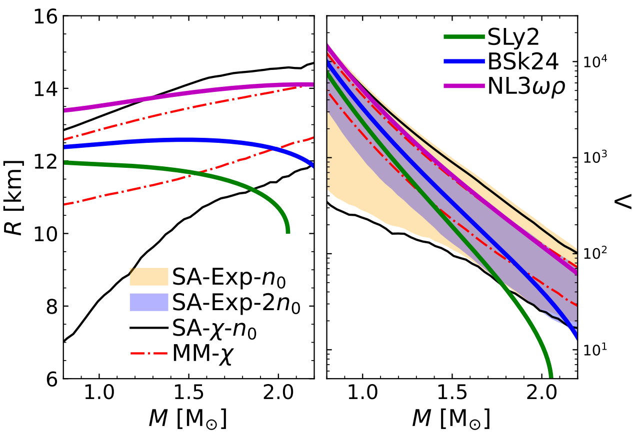

FIG. 2: Radius R and tidal deformability Λ as a function of the mass M (90 % contours) for the EoS sets discussed in this paper; the $M(R)$ and $M(\Lambda)$ sequence for EoSs RG(SLY2), PCP(BSK24) and GPPVA(NL3$\omega\rho$) (used as injection EoSs) are also presented in green, blue and magenta, respectively.

χ-EFT constraints) disfavor high and low pressures compared to SA-Exp-n_0 : the meta-model construction with its nucleonic hypothesis present a narrow δP in this density regime compared to piecewise polytropes that can explore a range of pressures up to two times larger. For semi-agnostic sets, extending the meta-model up to $n_{\text{match}} = 0.32$ fm^{-3} (SA-Exp-2n_0) results in tighter pressure contours in $n \in [n_0; 2n_0]$.

For $n > 2n_0$, the sets SA-Exp-n_0 , SA-Exp-2n_0 and SA-χ-n_0 offer a larger δP than MM-χ . In this density regime, the semi-agnostic sets allow for significantly softer core EoSs while in comparison the MM-χ presents particularly stiff EoS contours. The semi-agnostic sets indeed mimic well the presence of non-nucleonic degrees of freedom in the core of the star producing an overall softening of the EoS.

2. *Neutron-star astrophysical parameters*

In Fig. 2, we present the mass-radius and mass-tidal deformability 90% contours corresponding to the four EoS prior sets; the radius and tidal deformability ranges δR and $\delta\Lambda$ (on the 90% contours) explored by each set are presented in Table IV for various values of the total NS mass. The $M(R)$ and $M(\Lambda)$ sequences for the three injection EoSs RG(SLY2), PCP(BSK24) and GPPVA(NL3$\omega\rho$) are also presented in Fig. 2.

The full meta-model set MM-χ leads to the tighest contours in both $M(R)$ and $M(\Lambda)$, as expected by the EoS contours presented Fig. 1. The semi-agnostic set SA-Exp-2n_0 presents the second tighest contours out of the four sets, while the range explored by SA-Exp-n_0 and SA-χ-n_0 are quite similar. However, the set SA-χ-n_0 informed by χ-EFT data prefers slightly smaller radii and tidal deformabilities (more compact objects).

The injection EoS GPPVA(NL3$\omega\rho$) falls slightly outside or on the border of the 90% contours for all of the EoS sets in the range of very low mass NSs; this EoS is particularly stiff and leads to high radii and high tidal deformabilities. Similarly, the injection EoS RG(SLY2) steps outside of the 90% contours of the astrophysical parameter priors (for all the sets) when considering high mass NSs. Even though the injection nuclear parameters (see Table II) are within the prior interval presented in Table I, it does not garantee a large statistical realization of resembling EoSs and corresponding astrophysical parameters in semi-agnostic sets.

3. *Correlation between the pressure and nuclear parameters*

The Pearson correlation factors between NEPs and the β-equilibrated pressure (P_{pc}) as a function of the baryon density for the sets SA-Exp-n_0 and MM-χ are presented in Fig. 3.

In the low-density part of the outer crust ($n \lesssim 10^{-5}$ fm^{-3}), nuclei are almost isospin symmetric and E_{sat} dominates the contribution. The main pressure contribution in the outer crust is that of electrons: small values of E_{sat} imply small nucleus binding energy and small nuclei, which is why this parameter anti-correlates with the pressure. In the high density part of the outer crust ($10^{-5} \lesssim n \lesssim 4 \times 10^{-4}$ fm^{-3}), the nuclei in the lattice become more neutron rich: the symmetric matter energy correlates less with the pressure and E_{sym} starts to dominate the contribution (and to a lesser extent also K_{sym}).

In the low-density part of the inner crust ($4 \times 10^{-4} \lesssim n \lesssim 10^{-2}$ fm^{-3}), neutrons start dripping out of nuclei and contributing to the pressure, which is why the E_{sym} correlation with pressure drops significantly right after the outer–inner crust transition. The very low density of the neutron gas (much lower

Set	$\delta R(\mathrm{M}_\odot)$	$\delta R(1.4\,\mathrm{M}_\odot)$	$\delta R(2\,\mathrm{M}_\odot)$	$\delta\Lambda(\mathrm{M}_\odot)$	$\delta\Lambda(1.4\,\mathrm{M}_\odot)$	$\delta\Lambda(2\,\mathrm{M}_\odot)$
SA-Exp-n_0	5.06	3.87	3.23	5630	1194	174
SA-Exp-2n_0	2.72	2.57	2.47	3568	694	103
SA-χ-n_0	5.05	3.86	3.10	5244	1107	154
MM-χ	1.84	1.90	1.57	2685	548	76

TABLE IV: 90% contour radius and tidal deformability ranges $\delta R(M)$ (in km) and $\delta\Lambda(M)$ respectively, calculated at $M = 1, 1.4, 2\,\mathrm{M}_\odot$ for the EoS sets discussed in this paper.

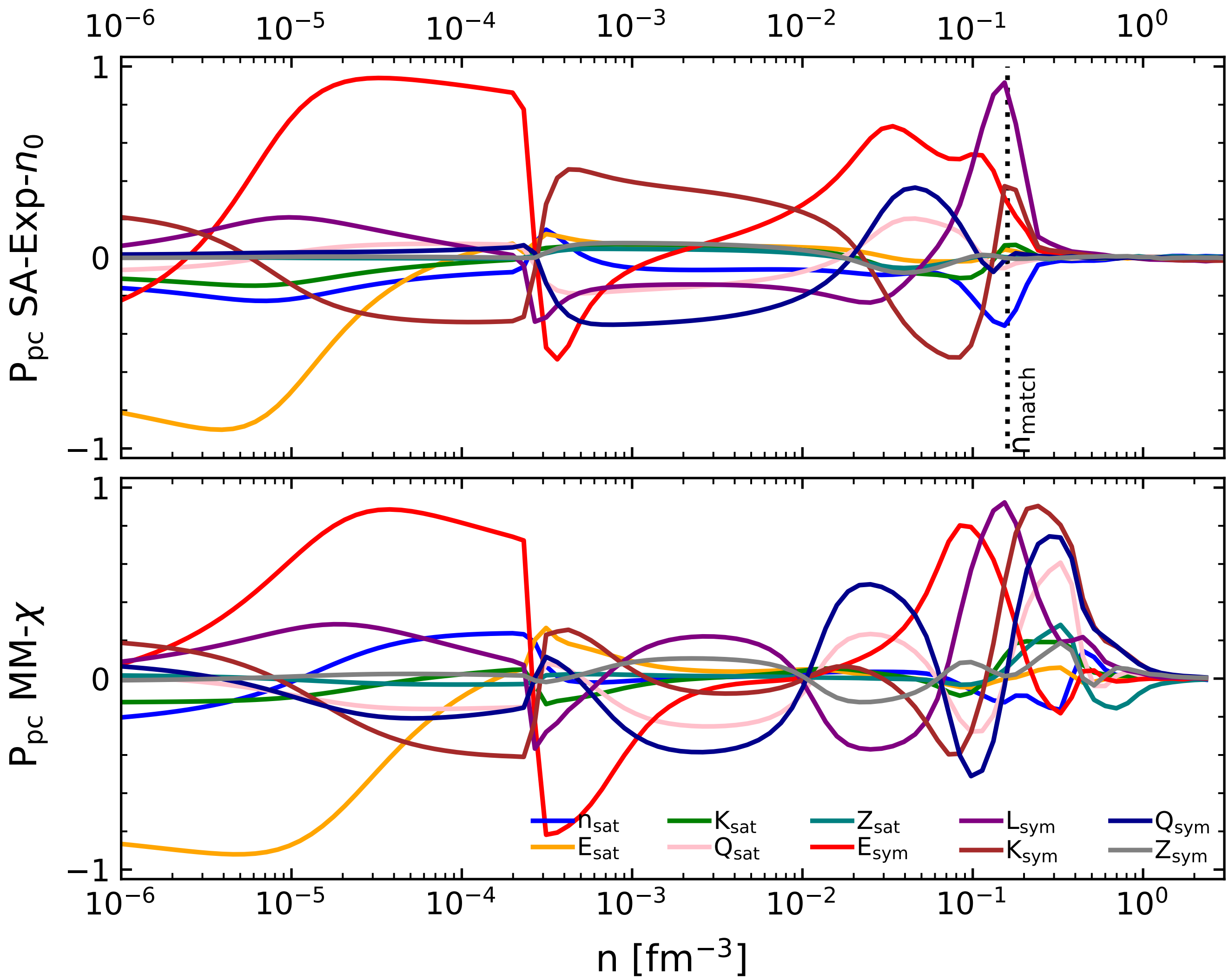

FIG. 3: Pearson correlation factors between the β-equilibrated pressure P_{pc} and the nuclear empirical parameters as a function of the baryon density n, for the sets SA-Exp-n_0 and MM-χ . For SA-Exp-n_0 , the matching density to polytropes is represented as a vertical dashed line.

than saturation density) also explains why the higher order parameters in the expansion, K_{sym} and Q_{sym} , take over the pressure contribution; as we progress deeper in the inner crust, the neutron-gas density increases and E_{sym} once again contributes significantly to the pressure. The χ-EFT calculations have a strong impact on K_{sym} and Q_{sym} in the low-density inner crust, acting as a decorrelating agent for those parameters.

In the density regime $10^{-2} \lesssim n \lesssim 10^{-1}$ fm^{-3} , the neutron gas presents densities similar to the ones of the clusters and E_{sym} dominates the pressure contribution: unbound neutrons are in a high-density environment and nuclei are also very neutron rich. Note that this region contains the core–crust transition for most of the models which is why a rapid evolution of many parameters is observed.

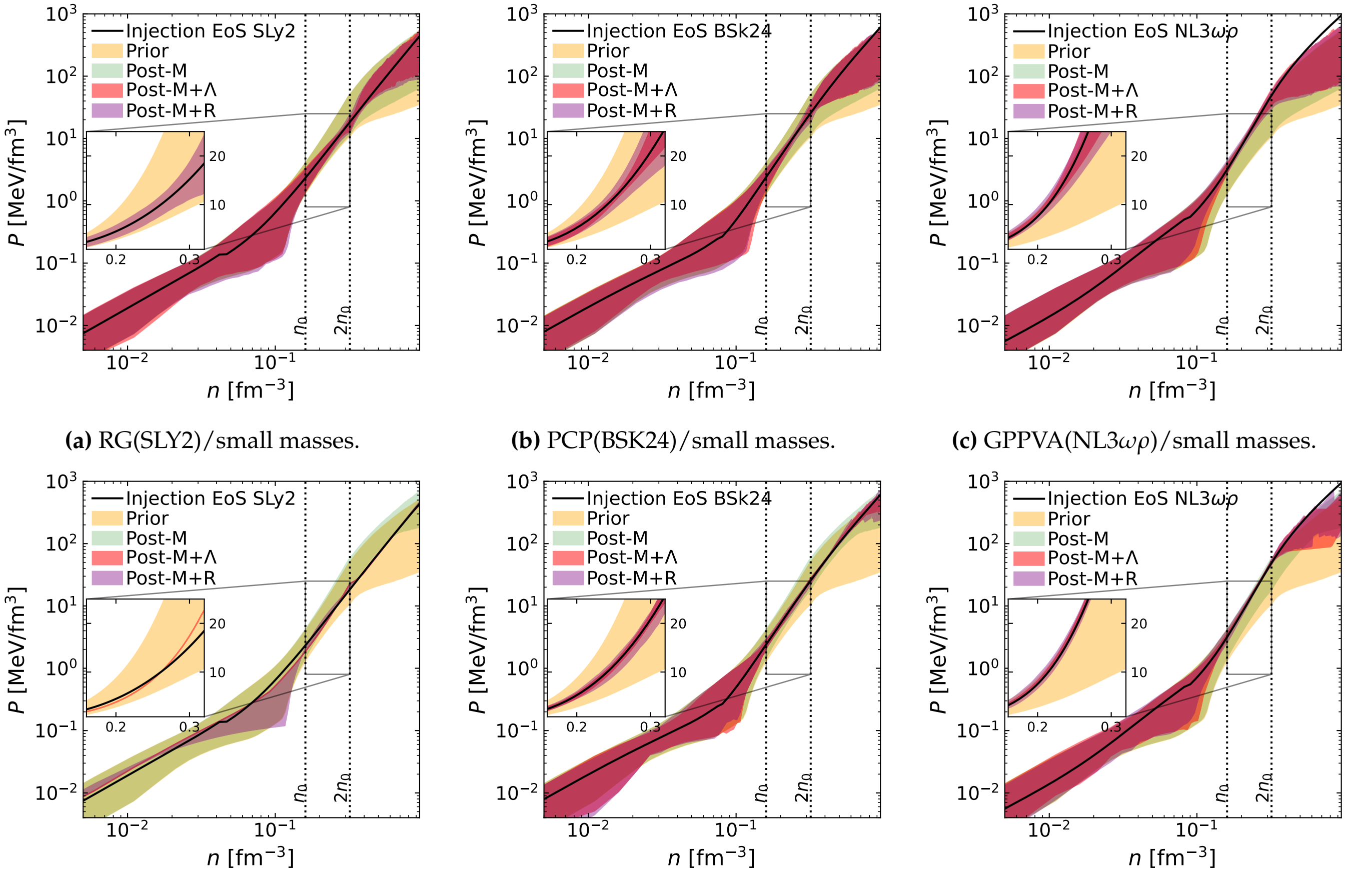

(a) RG(SLY2)/small masses. **(b)** PCP(BSK24)/small masses. **(c)** GPPVA(NL3$\omega\rho$)/small masses.

(d) RG(SLY2)/high masses. **(e)** PCP(BSK24)/high masses. **(f)** GPPVA(NL3$\omega\rho$)/high masses.

FIG. 4: Pressure P as a function of the baryon density n (90 % contours) for the prior SA-Exp-2n$_0$ (orange) and the posterior informed by the simulated detection of 10 NSs at 1% relative error of M (green), (M, Λ) (red) and (M, R) (purple). The injection EoSs (RG(SLY2), PCP(BSK24), and GPPVA(NL3$\omega\rho$)) are presented in black.

In the early core, a strong correlation between the pressure and L_{sym} appears: the pressure of pure neutron matter at nuclear saturation is solely determined by L_{sym} in the parabolic approximation to the symmetry energy; see Lattimer [51]. Isovector parameters L_{sym} , K_{sym} and Q_{sym} successively become the most important contribution to the pressure when the density in the core is increased, as per the Taylor expansion around saturation density the meta-model is based on. The correlation between the pressure and NEPs is extinguished quickly beyond $n = n_{\text{match}}$ for SA-Exp-n$_0$: NEPs influence minimally the pressure supported by polytropes, although the correlation is extended beyond n_{match}: this is because the value of the polytropic constant of the first polytrope of the agnostic construction is connected to the meta-model pressure at the match (see Sect. II A 2).

For MM-χ , even though the EoS is parametrized by the NEPs up to the highest densities, we observe a decrease and extinction of the correlation between the pressure and the nuclear parameters for $n \gtrsim 0.4$ fm^{-3} : different NEP combinations lead to the same pressure at very high density. This attests to an important degeneracy among the different NEPs in the building of the β-equilibrated pressure, particularly between the isoscalar and isovector sector. This is consistent with the findings of Iacovelli et al. [25], Mondal and Gulminelli [52]. Several parameters have a comparable importance in determining the β-equilibrated pressure, and this degeneracy challenges NEP's inference based on β-equilibrated pressure at high density.

B. Inference with simulated data

1. *Equation of state posteriors*

In Fig. 4, we present the EoS posteriors based on the set SA-Exp-2n$_0$ and informed by simulated small-mass NS sources and high-mass NS sources detections of M, $M - R$, and $M - \Lambda$ with 1% precision, for the three injection EoSs RG(SLY2), PCP(BSK24), and GPPVA(NL3$\omega\rho$).

The differences between the posteriors informed by

M, $M-R$ or $M-\Lambda$ detections show that the sole detection of the mass (in green) has the only effect of pushing the posterior towards high pressure values in the high-density regime, as expected. Indeed stiffer EoSs are needed to counterbalance gravity if the star is massive. $M-R$ (in purple) and $M-\Lambda$ (in red) simulated detections offer tight constraints in the density regime $n \in [n_0; 2n_0]$; the tidal (with the mass) detections provide slightly tighter constraints than the radius.

With regards to the posterior's ability to recover the injection EoS, for the PCP(BSK24) injection study, the posteriors tighten around the injection EoS well in all regimes of density for both small- and high-mass sources, as can be seen in Fig. 4b and Fig. 4e.

For the RG(SLY2) injection study, the simulated small-mass sources lead to posteriors recovering the injection EoS well in all regimes of density as can be seen in Fig. 4a. When considering high-mass sources as presented in Fig. 4d, the posterior is tight but does not recover the injection EoS. This can be understood with Fig. 2: the macroscopic parameters of high-mass NSs governed by the EoS RG(SLY2) lay outside the 90% contours of the prior; in other words our EoS prior sets do not sufficiently explore a part of the astrophysical parameter space, such that the inference encounters a lack of statistics when considering high masses. For example, when considering NS mass constraints applied to the set SA-Exp-2n$_0$, EoSs with a non-zero likelihood make only 45% of the total number of EoSs in the prior when high-mass neutron stars are considered (high mass NS can decimate the prior), whereas they make 98% when small neutron star masses are considered. A solution might be to employ semi-parametric EoSs with a high-density agnostic approach based on Gaussian Processes, which offer a much wider prior at high density (relevant for high-mass NSs), see Fig. 2 in Ref. [53] or to use more sophisticated Monte-Carlo methods to sample according to the likelihoods (Monte-Carlo Markov Chain, nested sampling etc.).

For the GPPVA(NL3$\omega\rho$) injection study, the posteriors informed by simulated small masses does not recover well the injection EoS in the high-density regime; however, it performs well for $n \lesssim 2n_0$, as presented in Fig. 4c.

Figure 4 highlights that guarantying that the NEP priors are wide enough to encompass all injection EoS NEPs, does not guarantee the realization of EoSs resembling the injection EoS in the prior with large statistics. However, for all injection EoSs in the case of the small-masses detections, the posteriors recover well the injection EoS in the intermediate density regime $n \leq 2n_0$, that is the regime of density of interest for NEP inference for this EoS set (SA-Exp-2n$_0$).

2. Nuclear parameter inference

Only few NEPs significantly correlate with the β-equilibrated pressure (see Fig. 3): $E_{\rm sat}$, $E_{\rm sym}$, $L_{\rm sym}$, $K_{\rm sym}$ and $Q_{\rm sym}$. $E_{\rm sat}$ significantly correlates with the pressure in a very low-density regime: constraining this parameter requires observations capable of constraining the pressure in the outer crust of the star, which is not the case for our simulated data. Given the results presented in Sect. III B 1, we restrict the NEP inference to that of $E_{\rm sym}$, $L_{\rm sym}$, $K_{\rm sym}$ and $Q_{\rm sym}$, based on small-masses $M-\Lambda$ simulated data. The prior distribution of NEPs $E_{\rm sym}$, $L_{\rm sym}$, $K_{\rm sym}$ and $Q_{\rm sym}$, as well as the posterior distributions informed by small-masses NSs simulations, are presented in Fig. 5 for $M-\Lambda$ detections). Additional results are shown for $M-R$ detections in Fig. 6 in Appendix A.

For $E_{\rm sym}$, the prior and astrophysically-informed posterior distributions for the sets SA-Exp-n$_0$ and SA-Exp-2n$_0$ coincide and are relatively flat (suggesting a uniform distribution similar to the NEP sampling)[4]. For the sets SA-χ-n$_0$ and MM-χ , the prior and astrophysically-informed posterior distributions are both peaked. We conclude that χ-EFT data imposed in $n \in [n_{\chi-\rm data}; n_0]$ lead to already peaked priors and that astrophysical constraints do not significantly peak the distribution; χ-EFT data applied for $n \geq n_0$ does not help constrain this parameter, in coherence with conclusions presented when discussing Fig. 1. Astrophysical information for small-masses simulations do not help recover the injection value of $E_{\rm sym}$.

For $L_{\rm sym}$ and $K_{\rm sym}$, astrophysical posteriors present more peaked distributions than priors for all the sets; the prior distributions are not uniform, as the meta-model construction in itself leads to NEP priors that depart from the NEP sampling. For $L_{\rm sym}$, the SA-Exp-2n$_0$ and MM-χ astrophysically-informed posteriors peak on the injection value for the injection EoS PCP(BSK24) (and to a lesser degree for RG(SLY2) and GPPVA(NL3$\omega\rho$)), suggesting that the density regime $n \in [n_0; 2n_0]$ plays a role in recovering $L_{\rm sym}$, as suggested in Fig. 3. For $K_{\rm sym}$, the MM-χ set presents a very peaked astrophysically-informed posterior distribution, systematically away from the injection value, suggesting that the extension of the meta-model EoS construction in the density regime $n \geq 2n_0$ pollutes the recovery of the injection value. This can be understood by the inability of the meta-model to reproduce well-known EoS models at high density (see discussion in Margueron et al. [26]), where higher orders of the Taylor expansion play an important role in the realization of the β-equilibrated pressure. The astrophysically-informed posteriors for the set SA-χ-n$_0$ resembles its prior. For SA-Exp-2n$_0$ in the RG(SLY2)

[4] The distributions presented in this section are drawn using a kernel density estimation.

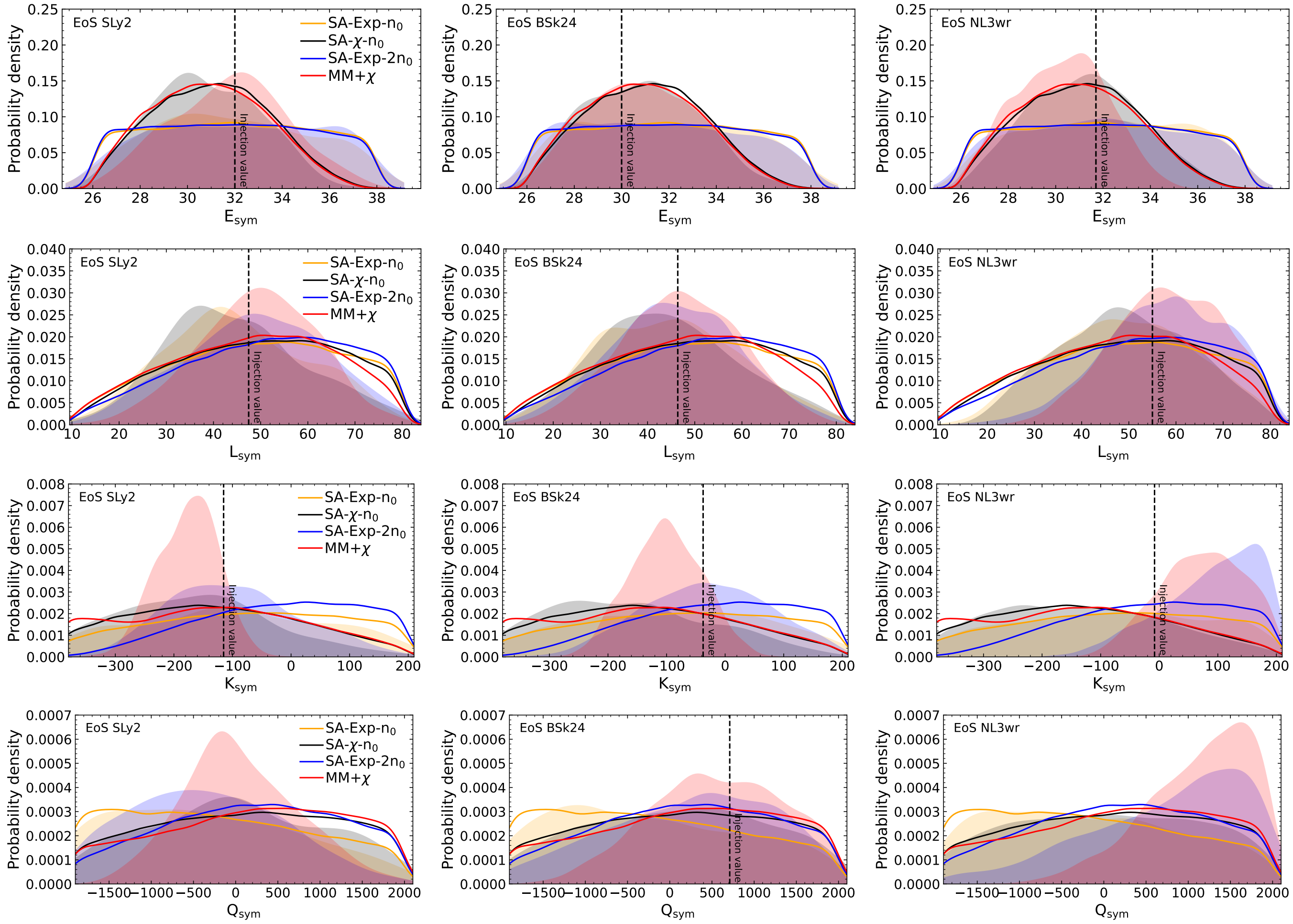

FIG. 5: $M-\Lambda$ informed posterior distribution for $E_{\rm sym}$, $L_{\rm sym}$, $K_{\rm sym}$ and $Q_{\rm sym}$ for small-mass NSs simulated with an uncorrelated bivariate Gaussian distibution with $\delta E = 0.01$. Results are presented for SA-Exp-n$_0$ in orange, SA-Exp-2n$_0$ in blue and MM-χ in red. For comparison, the prior distributions are shown with a plain line. The injection values of the NEPs for EoSs RG(SLY2), PCP(BSK24) and GPPVA(NL3$\omega\rho$) are represented as a vertical black dashed line.

and PCP(BSK24) injection studies, the posterior peaks on the injection value: we conclude that the density regime $n \in [n_0; 2n_0]$ plays an important role in constraining $K_{\rm sym}$, and that the semi-agnostic set SA-Exp-2n$_0$ is capable of recovering the injection value of the NEP, contrary to the MM-χ . The injection study with EoS GPPVA(NL3$\omega\rho$) however presents a peaked posterior distibution very far away from the injection value while it is shown in Fig. 4 that the β-equilibrated pressure with small-masses simulations is recovered well within the 90% contours for $n \in [n_0; 2n_0]$: this can be explained by the inability of the prior set SA-Exp-2n$_0$ to explore sufficiently the parameter space of NEPs. The injection-value point of GPPVA(NL3$\omega\rho$) for the $E_{\rm sym}$ -$K_{\rm sym}$ parameter space is located close to a region where the density lines present holes (or dips) in probability density. This suggests that while the boundaries for the uniform distribution samples of the NEPs (see Table I) encompasses the injection values of the NEPs, it does not garantee that the set of NEPs after the meta-model construction is uniformally distributed in the large dimensionality of the meta-model.

For $Q_{\rm sym}$ the MM-χ set presents the most peaked astrophysically-informed distributions. We note that injection value for $Q_{\rm sym}$ is only available for the EoS PCP(BSK24) and therefore conclusions on the recovery of the parameter throughout a large stiffness range is not possible in this study. However, the figure confirms that the density regime $n \geq 2n_0$ is very correlated to this parameter, which is a high-order parameter in the meta-model Taylor expansion.

IV. DISCUSSION

The semi-agnostic EoS construction presented in this paper can be amended to improve the statistical realization of NEP and EoS priors. In the future, we aim to include several improvements to `CUTER`. Concerning the high-density EoS, piecewise polytropes offer less flexibility than so-called non-parametric approaches like Gaussian Processes. The high-density flexibility of the EoS prior can be improved by using Gaussian Processes as high-density extension of our semi-agnostic approach; see Ng et al. [53]. This will improve the radius and tidal deformability recovery in the injection study for high-mass detections.

Moreover, in this paper, we used pre-computed sets of EoSs composed of 50000 EoSs each. Increasing the number of EoSs in the sets is a simple way to improve the smoothness of astrophysical posterior EoS contours. However, to obtain posteriors with a statistically significant number of EoS and NEP multi-dimensional realization, it may be necessary to produce EoSs concurrently with the Bayesian inference, that is to say generating EoSs according to the astrophysical detection likelihood with a smart sampler (also called sampling on the fly). We note that this would be incompatible with the current implementation of non-parametric high-density extensions.

Recently, an improved version of the meta-model construction was discussed in Lim and Schwenk [54]. It was also suggested that the higher order parameters could be resampled to improve the flexibility of the meta-model at high density and to ensure that the low-density behavior of the EoS does not impose any spurious correlation to the high-density regime (see e.g., Mondal and Gulminelli [55], Klausner et al. [56]). Amending the meta-model construction in our semi-agnostic models could improve the inference of NEPs, especially for high values of n_{match}.

The injection study could also be improved by employing more sophisticated simulations of astrophysical data. Taking into account the correlations of the astrophysical parameters in gravitational-wave and x-ray pulse-profile modeling, as well as the sensitivity of detectors such as Einstein Telescope/Cosmic Explorer or ATHENA, would clarify the capacity for NEP inference in the context of the next generation of telescopes.

V. CONCLUSION

In this paper, we explored the capability of semi-agnostic EoS priors to recover NEPs through injection studies based on three nucleonic EoSs and simple simulations of the mass, radius, and tidal deformability detection. We show that semi-agnostic priors with piecewise polytropes attached at $n = n_0, 2n_0$ offer a much better EoS flexibility than the full meta-model, in agreement also with previous findings (see e.g., Tews et al. [57] where speed-of-sound models were compared to a meta-model approach). Using injection studies based on nucleonic EoSs RG(SLY2), PCP(BSK24) and GPPVA(NL3$\omega\rho$), we show that astrophysical detections constrain the β-equilibrated pressure in different density regimes when small and high-mass detections of neutron stars are considered.

We point out that not all NEPs significantly correlate with the β-equilibrated pressure in regimes of densities relevant for astrophysical observations of the mass, radius and tidal deformability of NSs. We conclude that only a limited number of NEPs can be constrained by those astrophysical detections. We also show that semi-agnostic models can be more accurate to recover the injected K_{sym} than the full meta-model, as the later can present posterior distributions strongly peaked away from the injection value of the NEP. Finally, we discuss how to improve the EoS construction to ensure sufficient sampling in the NEP distribution and astrophysical parameter realization.

VI. ACKNOWLEDGMENTS

The authors thanks the developers of CUTER. L.S acknowledges the financial support of the National Science Foundation Grant No. PHY 21-16686. J.R. acknoledges support from the National Science Foundation Grant No. PHY 2409736. This work is supported by Deutsches Elektronen Synchrotron and Deutsches Centrum für Astrophysik. This work has been also partially supported by the IN2P3 Master Project MAC, and the CNRS International Research Project (IRP) 'Origine des éléments lourds dans l'univers: Astres Compacts et Nucléosynthèse (ACNu)'.

Appendix A: $M - R$ informed posterior distribution of NEPs

We find that the astrophysically informed posterior distribution are quite similar in the case of $M - R$ detections and $M - \Lambda$ detections. We find slightly more peaked distribution for E_{sym} and and L_{sym} when considering radius detection, and slightly less peaked distribution for K_{sym} informed by the radius than by the tidal deformability. This can be understood by the sensitivity of the radius on lower density regimes than tidal deformability, and by the fact that K_{sym} appears at a higher order in the meta-model Taylor expansion with respect to E_{sym} and L_{sym} .

[1] F. Özel and P. Freire, Annual Review of Astronomy and Astrophysics **54**, 401–440 (2016).

[2] E. Fonseca et al., The Astrophysical Journal Letters **915**, L12 (2021), arXiv:2104.00880 [astro-ph.HE].

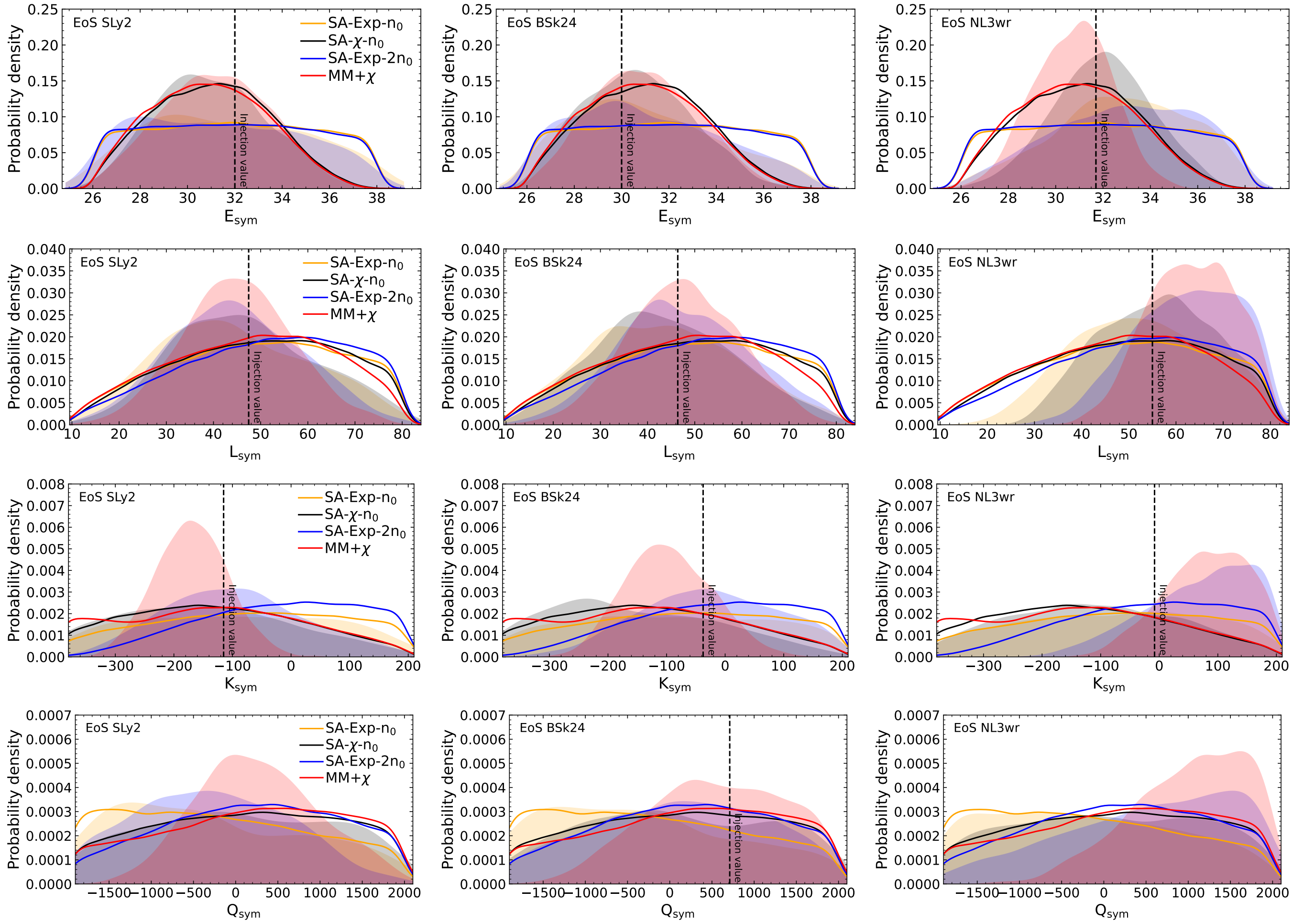

FIG. 6: $M-R$ informed posterior distribution for $E_{\rm sym}$, $L_{\rm sym}$, $K_{\rm sym}$ and $Q_{\rm sym}$ for small-mass NSs simulated with an uncorrelated bivariate Gaussian distibution with $\delta E = 0.01$. Results are presented for SA-Exp-n$_0$ in orange, SA-Exp-2n$_0$ in blue and MM-χ in red. For comparison, the prior distributions are shown with a plain line. The injection values of the NEPs for EoSs RG(SLY2), PCP(BSK24) and GPPVA(NL3$\omega\rho$) are represented as a vertical black dashed line.

[3] T. Dietrich, T. Hinderer, and A. Samajdar, General Relativity and Gravitation **53**, 27 (2021), arXiv:2004.02527 [gr-qc].

[4] B. P. Abbott, LIGO Scientific Collaboration, and Virgo Collaboration, Physical Review Letters **119**, 161101 (2017), arXiv:1710.05832 [gr-qc].

[5] B. P. Abbott, LIGO Scientific Collaboration, and Virgo Collaboration, Physical Review Letters **121**, 161101 (2018), arXiv:1805.11581 [gr-qc].

[6] R. Essick, P. Landry, and D. E. Holz, Phys. Rev. D **101**, 063007 (2020), arXiv:1910.09740 [astro-ph.HE].

[7] K. Chatziioannou, Gen. Rel. Grav. **52**, 109 (2020), arXiv:2006.03168 [gr-qc].

[8] T. Dietrich, M. W. Coughlin, P. T. H. Pang, M. Bulla, J. Heinzel, L. Issa, I. Tews, and S. Antier, Science **370**, 1450 (2020), arXiv:2002.11355 [astro-ph.HE].

[9] T. Wouters, P. T. H. Pang, H. Koehn, H. Rose, R. Somasundaram, I. Tews, T. Dietrich, and C. Van Den Broeck, Phys. Rev. D **112**, 043037 (2025), arXiv:2504.15893 [astro-ph.HE].

[10] A. L. Watts, N. Andersson, D. Chakrabarty, M. Feroci, K. Hebeler, G. Israel, F. K. Lamb, M. C. Miller, S. Morsink, F. Özel, A. Patruno, J. Poutanen, D. Psaltis, A. Schwenk, A. W. Steiner, L. Stella, L. Tolos, and M. van der Klis, Reviews of Modern Physics **88**, 021001 (2016), arXiv:1602.01081 [astro-ph.HE].

[11] T. E. Riley, A. L. Watts, S. Bogdanov, P. S. Ray, R. M. Ludlam, S. Guillot, Z. Arzoumanian, C. L. Baker, A. V. Bilous, D. Chakrabarty, K. C. Gendreau, A. K. Harding, W. C. G. Ho, J. M. Lattimer, S. M. Morsink, and T. E. Strohmayer, The Astrophysical Journal **887**, L21 (2019).

[12] M. C. Miller, F. K. Lamb, A. J. Dittmann, S. Bogdanov, Z. Arzoumanian, K. C. Gendreau, S. Guillot, A. K. Harding, W. C. G. Ho, J. M. Lattimer, R. M. Ludlam, S. Mahmoodifar, S. M. Morsink, P. S. Ray, T. E. Strohmayer, K. S. Wood, T. Enoto, R. Foster, T. Okajima, G. Prigozhin, and Y. Soong, Astrophysical Journal, Letters **887**, L24 (2019), arXiv:1912.05705 [astro-ph.HE].

[13] T. E. Riley, A. L. Watts, P. S. Ray, S. Bogdanov, S. Guillot, S. M. Morsink, A. V. Bilous, Z. Arzoumanian, D. Choudhury, J. S. Deneva, K. C. Gendreau, A. K. Harding, W. C. G. Ho, J. M. Lattimer, M. Loewenstein, R. M. Ludlam, C. B. Markwardt, T. Okajima, C. Prescod-Weinstein, R. A. Remillard, M. T. Wolff, E. Fonseca, H. T.

Cromartie, M. Kerr, T. T. Pennucci, A. Parthasarathy, S. Ransom, I. Stairs, L. Guillemot, and I. Cognard, Astrophysical Journal, Letters **918**, L27 (2021), arXiv:2105.06980 [astro-ph.HE].

[14] M. C. Miller, F. K. Lamb, A. J. Dittmann, S. Bogdanov, Z. Arzoumanian, K. C. Gendreau, S. Guillot, W. C. G. Ho, J. M. Lattimer, M. Loewenstein, S. M. Morsink, P. S. Ray, M. T. Wolff, C. L. Baker, T. Cazeau, S. Manthripragada, C. B. Markwardt, T. Okajima, S. Pollard, I. Cognard, H. T. Cromartie, E. Fonseca, L. Guillemot, M. Kerr, A. Parthasarathy, T. T. Pennucci, S. Ransom, and I. Stairs, Astrophysical Journal, Letters **918**, L28 (2021), arXiv:2105.06979 [astro-ph.HE].

[15] D. Choudhury, T. Salmi, S. Vinciguerra, T. E. Riley, Y. Kini, A. L. Watts, B. Dorsman, S. Bogdanov, S. Guillot, P. S. Ray, D. J. Reardon, R. A. Remillard, A. V. Bilous, D. Huppenkothen, J. M. Lattimer, N. Rutherford, Z. Arzoumanian, K. C. Gendreau, S. M. Morsink, and W. C. G. Ho, The Astrophysical Journal Letters **971**, L20 (2024), arXiv:2407.06789 [astro-ph.HE].

[16] B. P. Abbott, L. S. Collaboration), J. Harms, et al., Classical and Quantum Gravity **34**, 044001 (2017).

[17] D. Reitze, R. X. Adhikari, S. Ballmer, B. Barish, L. Barsotti, G. Billingsley, D. A. Brown, Y. Chen, D. Coyne, R. Eisenstein, M. Evans, P. Fritschel, E. D. Hall, A. Lazzarini, G. Lovelace, J. Read, B. S. Sathyaprakash, D. Shoemaker, J. Smith, C. Torrie, S. Vitale, R. Weiss, C. Wipf, and M. Zucker, "Cosmic explorer: The u.s. contribution to gravitational-wave astronomy beyond ligo," (2019), arXiv:1907.04833 [astro-ph.IM].

[18] M. Evans et al., arXiv e-prints , arXiv:2109.09882 (2021), arXiv:2109.09882 [astro-ph.IM].

[19] M. Punturo, M. Abernathy, F. Acernese, B. Allen, N. Andersson, K. Arun, F. Barone, B. Barr, M. Barsuglia, M. Beker, N. Beveridge, S. Birindelli, S. Bose, L. Bosi, S. Braccini, C. Bradaschia, T. Bulik, E. Calloni, G. Cella, E. Chassande Mottin, S. Chelkowski, A. Chincarini, J. Clark, E. Coccia, C. Colacino, J. Colas, A. Cumming, L. Cunningham, E. Cuoco, S. Danilishin, K. Danzmann, G. De Luca, R. De Salvo, T. Dent, R. De Rosa, L. Di Fiore, A. Di Virgilio, M. Doets, V. Fafone, P. Falferi, R. Flaminio, J. Franc, F. Frasconi, A. Freise, P. Fulda, J. Gair, G. Gemme, A. Gennai, A. Giazotto, K. Glampedakis, M. Granata, H. Grote, G. Guidi, G. Hammond, M. Hannam, J. Harms, D. Heinert, M. Hendry, I. Heng, E. Hennes, S. Hild, J. Hough, S. Husa, S. Huttner, G. Jones, F. Khalili, K. Kokeyama, K. Kokkotas, B. Krishnan, M. Lorenzini, H. Lück, E. Majorana, I. Mandel, V. Mandic, I. Martin, C. Michel, Y. Minenkov, N. Morgado, S. Mosca, B. Mours, H. Müller–Ebhardt, P. Murray, R. Nawrodt, J. Nelson, R. Oshaughnessy, C. D. Ott, C. Palomba, A. Paoli, G. Parguez, A. Pasqualetti, R. Passaquieti, D. Passuello, L. Pinard, R. Poggiani, P. Popolizio, M. Prato, P. Puppo, D. Rabeling, P. Rapagnani, J. Read, T. Regimbau, H. Rehbein, S. Reid, L. Rezzolla, F. Ricci, F. Richard, A. Rocchi, S. Rowan, A. Rüdiger, B. Sassolas, B. Sathyaprakash, R. Schnabel, C. Schwarz, P. Seidel, A. Sintes, K. Somiya, F. Speirits, K. Strain, S. Strigin, P. Sutton, S. Tarabrin, A. Thüring, J. van den Brand, C. van Leewen, M. van Veggel, C. van den Broeck, A. Vecchio, J. Veitch, F. Vetrano, A. Vicere, S. Vyatchanin, B. Willke, G. Woan, P. Wolfango, and K. Yamamoto, Classical and Quantum Gravity **27**, 194002 (2010).

[20] S. Hild et al., Classical and Quantum Gravity **28**, 094013 (2011), arXiv:1012.0908 [gr-qc].

[21] M. Branchesi et al., Journal of Cosmology and Astroparticle Physics **2023**, 068 (2023), arXiv:2303.15923 [gr-qc].

[22] B. P. Abbott, (LIGO Scientific Collaboration, and J. Harms, Classical and Quantum Gravity **34**, 044001 (2017), arXiv:1607.08697 [astro-ph.IM].

[23] K. Nandra et al., arXiv e-prints , arXiv:1306.2307 (2013), arXiv:1306.2307 [astro-ph.HE].

[24] W. D. Myers and W. J. Swiatecki, Annals of Physics **55**, 395 (1969).

[25] F. Iacovelli, M. Mancarella, C. Mondal, A. Puecher, T. Dietrich, F. Gulminelli, M. Maggiore, and M. Oertel, Physical Review D **108**, 122006 (2023), arXiv:2308.12378 [gr-qc].

[26] J. Margueron, R. Hoffmann Casali, and F. Gulminelli, Physical Review C **97**, 025805 (2018), arXiv:1708.06894 [nucl-th].

[27] S. M. A. Imam, A. Mukherjee, B. K. Agrawal, and G. Banerjee, Phys. Rev. C **109**, 025804 (2024), arXiv:2305.11007 [nucl-th].

[28] Z. Zhu and R. O'Shaughnessy, arXiv e-prints , arXiv:2508.11875 (2025), arXiv:2508.11875 [astro-ph.HE].

[29] P. J. Davis, H. Dinh Thi, A. F. Fantina, F. Gulminelli, M. Oertel, and L. Suleiman, Astronomy & Astrophysics **687**, A44 (2024), arXiv:2406.14906 [astro-ph.HE].

[30] P. J. Davis, H. Dinh Thi, A. F. Fantina, F. Gulminelli, M. Oertel, and L. Suleiman, "Cuter (crust unified tool for equation-of-state reconstruction)," (2024).

[31] T. Carreau, F. Gulminelli, and J. Margueron, European Physical Journal A **55**, 188 (2019), arXiv:1902.07032 [nucl-th].

[32] M. Wang, W. J. Huang, F. G. Kondev, G. Audi, and S. Naimi, Chinese Physics C **45**, 030003 (2021).

[33] C. Drischler, K. Hebeler, and A. Schwenk, Physical Review C **93**, 054314 (2016), arXiv:1510.06728 [nucl-th].

[34] S. Huth et al., Nature **606**, 276 (2022), arXiv:2107.06229 [nucl-th].

[35] I. Vidaña, in Journal of Physics Conference Series, Journal of Physics Conference Series, Vol. 668 (IOP, 2016) p. 012031, arXiv:1509.03587 [nucl-th].

[36] M. Oertel, F. Gulminelli, C. Providência, and A. R. Raduta, European Physical Journal A **52**, 50 (2016), arXiv:1601.00435 [nucl-th].

[37] G. Baym, T. Hatsuda, T. Kojo, P. D. Powell, Y. Song, and T. Takatsuka, Reports on Progress in Physics **81**, 056902 (2018), arXiv:1707.04966 [astro-ph.HE].

[38] J. S. Read, B. D. Lackey, B. J. Owen, and J. L. Friedman, Physical Review D **79**, 124032 (2009), arXiv:0812.2163 [astro-ph].

[39] M. Oertel, M. Hempel, T. Klähn, and S. Typel, Reviews of Modern Physics **89**, 015007 (2017), arXiv:1610.03361 [astro-ph.HE].

[40] A. Le Fèvre, Y. Leifels, W. Reisdorf, J. Aichelin, and C. Hartnack, Nuclear Physics A **945**, 112 (2016), arXiv:1501.05246 [nucl-ex].

[41] P. Danielewicz, R. Lacey, and W. G. Lynch, Science **298**, 1592 (2002), arXiv:nucl-th/0208016 [nucl-th].

[42] R. C. Tolman, Physical Review **55**, 364 (1939).

[43] J. R. Oppenheimer and G. M. Volkoff, Physical Review **55**, 374 (1939).

[44] T. Hinderer, Astrophyical Journal **677**, 1216 (2008), arXiv:0711.2420 [astro-ph].

[45] S. Typel et al., "Compose reference manual," (2022).
[46] F. Gulminelli and A. R. Raduta, Phys. Rev. C **92**, 055803 (2015), arXiv:1504.04493 [nucl-th].
[47] J. M. Pearson, N. Chamel, A. Y. Potekhin, A. F. Fantina, C. Ducoin, A. K. Dutta, and S. Goriely, MNRAS **481**, 2994 (2018), [Erratum: MNRAS 486, 768 (2019)], arXiv:1903.04981 [astro-ph.HE].
[48] F. Grill, H. Pais, C. Providência, I. Vidaña, and S. S. Avancini, Phys. Rev. C **90**, 045803 (2014), arXiv:1404.2753 [nucl-th].
[49] A. Boudon, H. Qi, J.-F. Coupechoux, P. Landry, and V. Sordini, arXiv e-prints , arXiv:2501.11585 (2025), arXiv:2501.11585 [gr-qc].
[50] P. Virtanen and SciPy 1.0 Contributors, Nature Methods **17**, 261 (2020).
[51] J. M. Lattimer, Nuclear Physics A **928**, 276 (2014).
[52] C. Mondal and F. Gulminelli, Phys. Rev. D **105**, 083016 (2022), arXiv:2111.04520 [nucl-th].
[53] S. Ng, I. Legred, L. Suleiman, P. Landry, L. Traylor, and J. Read, Classical and Quantum Gravity **42**, 205008 (2025).
[54] Y. Lim and A. Schwenk, Phys. Rev. C **109**, 035801 (2024).
[55] C. Mondal and F. Gulminelli, Phys. Rev. C **107**, 015801 (2023), arXiv:2209.05177 [nucl-th].
[56] P. Klausner, M. Antonelli, and F. Gulminelli, (2025), arXiv:2505.16929 [nucl-th].
[57] I. Tews, J. Margueron, and S. Reddy, Phys. Rev. C **98**, 045804 (2018), arXiv:1804.02783 [nucl-th].